MDPI

Article

Nitrogen Doped Cobalt Anchored on the Used Resin-Based Catalyst to Activate Peroxymonosulfate for the Removal of Ibuprofen

Cheng Wang [1], Guangzhen Zhou [1], Yanhua Xu [1], Peng Yu [1] and Yongjun Sun [2,*]

[1] School of Environmental Science and Engineering, Nanjing Tech University, Nanjing 211816, China
[2] College of Urban Construction, Nanjing Tech University, Nanjing 211816, China
* Correspondence: sunyongjun@njtech.edu.cn

Abstract: The ion exchange resin is mainly composed of carbon, and it can form carbon material after calcination in the isolation of oxygen. Meanwhile, the nitrogen doping of metal-based carbon materials has attracted extensive attention in activating peroxymonosulfate (PMS) to produce active groups in the degradation of refractory organic pollutants. In this study, the used D001 resin served as the source of carbon material and catalyst carrier, cobalt ions adsorbed by impregnation, and then mixed with dicyandiamide and carbon balls formed by calcined (N-Co/D001CB). After nitrogen doping, cobalt exists in the form of cobalt sulfide with high crystallinity, and the serious problems of skeleton shrinkage and internal blockage are significantly alleviated. Under certain catalytic reaction conditions, the degradation rate of ibuprofen in one hour was more than 95%, which was significantly higher than that of cobalt. Finally, quenching experiments found that $SO_4^-\cdot$ is the main pathway for pollutant degradation, followed by $\cdot OH$, and there also exists the contributions of $\cdot O_2^-$ and $^1O_2$. In summary, the catalyst was prepared easily and had efficient catalytic activity, but it also recycled its resources with a low disposal cost of used D001CB, realizing the purpose of recycling waste materials and applying them in pollutant treatment.

Keywords: used D001 resin; cobalt sulfide; carbon materials; peroxymonosulfate

1. Introduction

Ibuprofen, as a kind of pharmaceutical and personal care product (PPCP), is widely used and discharged into the environment, and it tends to be persistent, as well as bioaccumulated organic pollutants due to its poor self-decomposition ability, which is doubtless harmful to the ecological environment and human health [1–3]. However, PPCPs are hard to separate or degrade by traditional treatment methods and often use advanced oxidation processes (AOPs) instead, such as O_3, Fenton, Fenton-like, and photocatalysts [4–6]. Among them, activating PMS by heterogeneous catalyst materials to produce sulfate radicals ($SO_4^-\cdot$) has a splendid effect on the removal of refractory pollutants [7,8]. In the process of activating PMS to degrade organic matter, a variety of radical or nonradical active components can be produced, and the contribution degree varies. In radical systems, $SO_4^-\cdot$ often plays the largest role, while $^1O_2$ is a nonradical function, which regularly depends on completely different activation methods and catalyst materials [9–11].

Many carbon materials, such as carbon nanotubes (CNTs) [12], reduced graphene oxides (rGOs) [13], biochars [14], and nitrogen/sulfur-doped carbon [15], due to their large surface area, good stability, good inherent properties, abundant sources, and low price, have attracted extensive attention [16], and they are often combined with transition metals to synthesize heterogeneous supported catalysts in the activation of PDS/PMS [17]. In various heterogeneous transition metal-connected catalysts, metal cobalt has a high standard electrode potential and is close to that of PMS [18], the preparation of cobalt-containing oxides [19], sulfides [20], and hydroxides [21]. or composites with other materials have an

excellent ability to activate PMS [22,23]. Significantly, cobalt-supported carbon material often plays an advantage in the interaction between metal and carrier to promote catalytic activity with low dissolution of cobalt ions [24]. D001 resin, consisting of -SO$_3$H groups regarded as a source of carbon material, has a favorable ability for ion exchange [25], which efficiently achieves the purpose of metal ion separation in water and forms a spherical structure after calcining. The used D001 resin that adsorbed the calcium or magnesium ions in the soft water treatment was selected as the carrier to prepare the catalyst, so that it greatly reduces the disposal cost of the used D001 resin as well as realizes its resource utilization. Unfortunately, in previous published studies [26], carbonized material still has serious problems with shrinkage of the resin skeleton and blockage of internal pores, which inevitably affect its catalytic performance and utilization ratio of metal components. Studies have found that nitrogen-doped metal-based carbon materials realized from the dicyandiamide (DCD) pyrolysis process can control the agglomeration of internal mental particles and form rich metal nitrogen sites [27], as well as increase the specific surface area of materials [28,29], which may be a certain reference value for responding to the above problems.

Over the years, nitrogen-doped carbon materials composed of active parts and supports have been widely studied. Combined with the application of transition metal-based carbon materials in advanced oxidation processes, nitrogen species can enhance the dispersion and stability of metal on materials [3] and modify their oxidoreduction properties. Relevant analysis has shown that the Lewis basic sites in carbon catalysts possess a superior capability to redox procedures [30]; meanwhile, existing N species (such as graphitic N, pyrrolic N, and pyridinic N) will break the structural inertia of the carbon used for electron transfer, improve the electronic state of the carbon catalyst associated with the electron acceptor molecule, and help improve the catalytic performance [2,31]. However, the separation and recycling of catalysts continues to be a vital downside when they eventually enter the water reaction system in the form of powder. This is an urgent problem to be solved, which also limits its application in practical engineering.

Given the above discussion, nitrogen-doped and cobalt-based carbon materials indeed have a great catalytic effect on activating PMS, and the design of a nitrogen-doped cobalt-supported used D001 resin carbon ball catalyst was expected to address the disposal problems of used D001 resin and resource utilization, material finalization, synchronous nitrogen doping, as well as overcoming the serious shrinkage of the skeleton and blockage of pores. Relevant experiments found that, among several nitrogen-containing substances, the mixed sintering of DCD and resin improved its specific surface area and catalytic activity and realized nitrogen doping of the material. In this study, the used D001 resin acted as the carbon source and the carrier of metal cobalt. When cobalt ions were adsorbed and mixed with DCD, a black carbon ball catalyst formed after being calcined in a tubular furnace for several hours. The morphology, composition, and valence of the elements were studied through relevant characterization, and their catalytic activity was investigated through a degradation experiment of ibuprofen by activating PMS. The effects of other experimental conditions on the degradation process and the stability of the materials were discussed. Next, the degradation mechanism and the causes of the assorted influencing factors were analyzed through radical quenching experiments combined with relevant EPR characterization and existing research analysis. Finally, the degradation path of IBU was inferred according to LC-MS analysis and combined with relevant studies. Overall, the composite carbon material catalyst based on the used D001 resin can mitigate its disposal and resource waste problems and can be used as a reference for resource utilization of waste carbon materials.

2. Materials and Methods

2.1. Materials and Instruments

(1)　Main drugs and reagents: Used D001 resin (Jinkai resin company, Yancheng, China), Dicyandiamide (DCD, CAS: 461-58-5, AR, Yatai chemical reagent), Ibuprofen (IBU,

CAS: 15687-27-1, Shanghai aladdln biochemical technology), Peroxymonosulfate (KHSO$_5$, CAS: 70693-62-8, 45%, Sinopharm chemical reagent), Cobalt nitrate hexahydrate (CAS: 10026-22-9, AR, Sinopharm chemical reagent), Phosphoric acid (CAS: 7664-38-2, AR, Sinopharm chemical reagent), Methanol (MeOH, CAS: 67-56-1, AR, Sinopharm chemical reagent), Acetonitrile (CAS: 75-05-8, BR, TEDIA), Ethanol (Eth, CAS: 64-17-5, AR, Sinopharm chemical reagent), Tert butyl alcohol (TBA, CAS: 75-65-0, AR, Sinopharm chemical reagent), L-histidine (L-his, CAS: 71-00-1, AR, Sinopharm chemical reagent), Furfuryl alcohol (FFA, CAS: 98-00-0, AR, China Huixing biochemical reagent), p-BenzoQuinone (p-BQ, CAS: 106-51-4, 99%, Shanghai aladdln biochemical technology), Sodium bicarbonate (CAS: 144-55-8, GR, Nanjing chemical reagent), Anhydrous sodium sulfate (CAS: 7757-82-6, AR, Sinopharm chemical reagent), Sodium dihydrogen phosphate (CAS: 13472-35-0, AR, Shanghai Lingfeng chemical reagent), Sodium chloride (CAS: 7647-14-5, AR, Xilong scientific and chemical experimental reagent), etc.

(2) Main instruments: Water bath thermostatic oscillator, Thermostatic drying oven, Tubular furnace, High-performance liquid chromatograph (HPLC), Total organic carbon analyzer (TOC), Liquid chromatography mass spectrometer (LC-MS), Inductively coupled plasma optical emission spectrometry (ICP-OES), Scanning electron microscope (SEM), Electron emission spectrometer (EDS), Transmission scanning electron microscope (TEM), X-ray diffractometer (XRD), Fourier transform infrared (FT-IR). X-ray photoelectron spectroscopy (XPS), Brunauer Emmett Teller (BET), and electron paramagnetic resonance spectroscopy (EPR) were performed.

2.2. N-Co/D001CB Catalyst Preparation

The used D001 resin was washed in a conical flask containing ethanol or water and oscillated for some time at an ambient temperature several times until the laundry water was clear. Then, the resin was separated from the water and dried. Next, the resin was adsorbed with a definite quantity of cobalt ions and mixed with dicyandiamide (DCD). According to a series of experimental optimizations, the following preparation methods were obtained. Adsorbing a certain amount (0.25 mmol–1.25 mmol) of Co^{2+} solution per gram of used resin, with a solid–liquid ratio of 1 g: 20 mL. After shaking for two hours in an oscillator, the resin was removed, regularly mixed with DCD, and then dried in an oven. The above arid resin was transferred into a tubular furnace, heated to 550 °C, and kept for 6 h at a heating rate of 5 °C/min. The carbon ball formed by calcination was N-Co/D001CB.

The content fraction of cobalt in the catalyst was marked by the theoretical calculation of the ratio of the adsorption amount of cobalt to the mass of the carbon balls. To distinguish it from other materials, the carbon ball prepared from D001 resin and sintered with a nitrogenous component under optimal conditions was named N-Co/D001CB. Similarly, according to the different components added in the preparation process, there can be the following materials: carbonized used D001 resin (D001CB), carbonized cobalt anchored used D001 resin (Co/D001CB), used D001 resin carbonized with DCD (N-Co/D001CB), used D001 resin adsorbed cobalt ion, and carbonized with DCD (N-Co/D001CB).

2.3. Characterization and Analytical Method

The characterization and analytical methods of N-Co/D001CB refer to the team's previous studies of Co/D001CB [26].

2.4. Catalytic Activity Study

The catalytic activity of the N-Co/D001CB catalyst was tested by a degradation experiment with 10 mg/L ibuprofen (IBU) conducted in an oscillating conical flask with 50 mL of the reaction liquid. At the reaction time, a 2 mL water sample was taken and quickly filtered through a 0.22 μm filter membrane into a sample bottle containing 20 μL of methanol every 10 min and detected by HPLC under a 221 nm detection wavenumber.

Based on the testing methods, the concentration of the standard solution had an extremely high linear correlation with the measured peak area, and the value of R^2 was 0.9997. Pre-experiments have shown that carbon ball materials alone have little ability in the adsorption of IBU, and then catalytic activation in various systems and different kinds of N-Co/D001CB were discussed. The effects of other reaction conditions (such as catalyst loading, temperature, and pH value) were similarly explored. Simultaneously, the cobalt ion leaching and recycling of the material were also investigated under optimal conditions. A variety of capture agents are used to trap possible free radicals and non-free radicals [32,33]. Combined with EPR, the action mechanism of the active species was verified again to explain some strange experimental phenomena. Finally, the possible degradation pathway was inferred according to the main molecular weight, according to the LC-MS results.

3. Results and Discussion

### 3.1. Material Characterization of N-Co/D001CB Catalyst

The material morphology photograph under the characterization of SEM and the corresponding EDS element-layered images are shown in Figure 1, and their microstructure was examined by TEM (Figure 2). More surface topography and results are shown in Figure S1. There were several different features between them. The carbon ball (Figure 1a,b) was relatively intact and flat, which represents D001CB and Co/D001CB, while N-Co/D001CB has obvious rupture, and the surface became uneven (Figure 1c). It can be seen from D001CB that there are a large number of lumps and long strips distributed on the carbon ball, which are the corresponding magnesium sulfides or oxides in combination with element mapping. In contrast, the dense small particulate matter grows on the surface Co/D001CB, and it was difficult to see small pores on the surface, so the metal cobalt complex in the internal or surface formation of small particles blocks the pore channel. More importantly, a large number of granular objects attached to N-Co/D001CB with the surface structure of rupture and unevenness resulting from sintering with DCD improved its specific surface area and alleviated shrinkage of the resin skeleton, causing its rupture, which also greatly increased the distribution and exposure area of the cobalt complex in the internal carbon ball. Compared with the TEM of N/D001CB in Figure 2a, there are a lot of black spots on the N-Co/D001CB morphology according to Figure 2b, which may be the corresponding metal compound formed by metal cobalt on the carbon ball. In addition, it can be clearly found that there are many hollows in Figure 2c, signifying the pore structure on the material, and the metal cobalt components are uniformly distributed on the material.

It can be seen from the XRD patterns that all carbon sphere materials have typical amorphous carbon peaks at a 2θ value of about 23° [34,35]. When carbonized with the used D001 resin, diffraction peaks appeared at diffraction angles of 42.9° and 62.4°, which may be the magnesium oxide formed, corresponding to the (200) and (220) crystal planes of magnesium (JCPDS: 45-0946). Comparing Figure 3 with Figure S2, whether the cobalt loading materials are calcined with DCD or not, the positions of the XRD diffraction peaks are similar, and all of them have four obvious diffraction peaks. With an increase in cobalt content, their intensity increases. It is worth noting that N-Co/D001CB both had sharper and narrower peaks, and there were three additional diffraction peaks with low intensity, but Co/D001CB did not show these peaks. After crystal form analysis, the characteristic diffraction peak positions at diffraction angles at 30.5°, 35.2°, 47.7°, 54.5°, 62.3°, 66.3°, and 74.5° correspond to the crystal planes of (100), (101), (102), (110), (103), (201), and (202), respectively, on the standard card JCPDS:48-0826 and represent the material of CoS [36,37]. Above all, the resin calcined with DCD can greatly improve the crystallinity of the formed CoS instead of changing the existing form on the carbon balls, which contributes to exposing more metal-active component crystal planes in the reaction system to improve its catalytic performance.
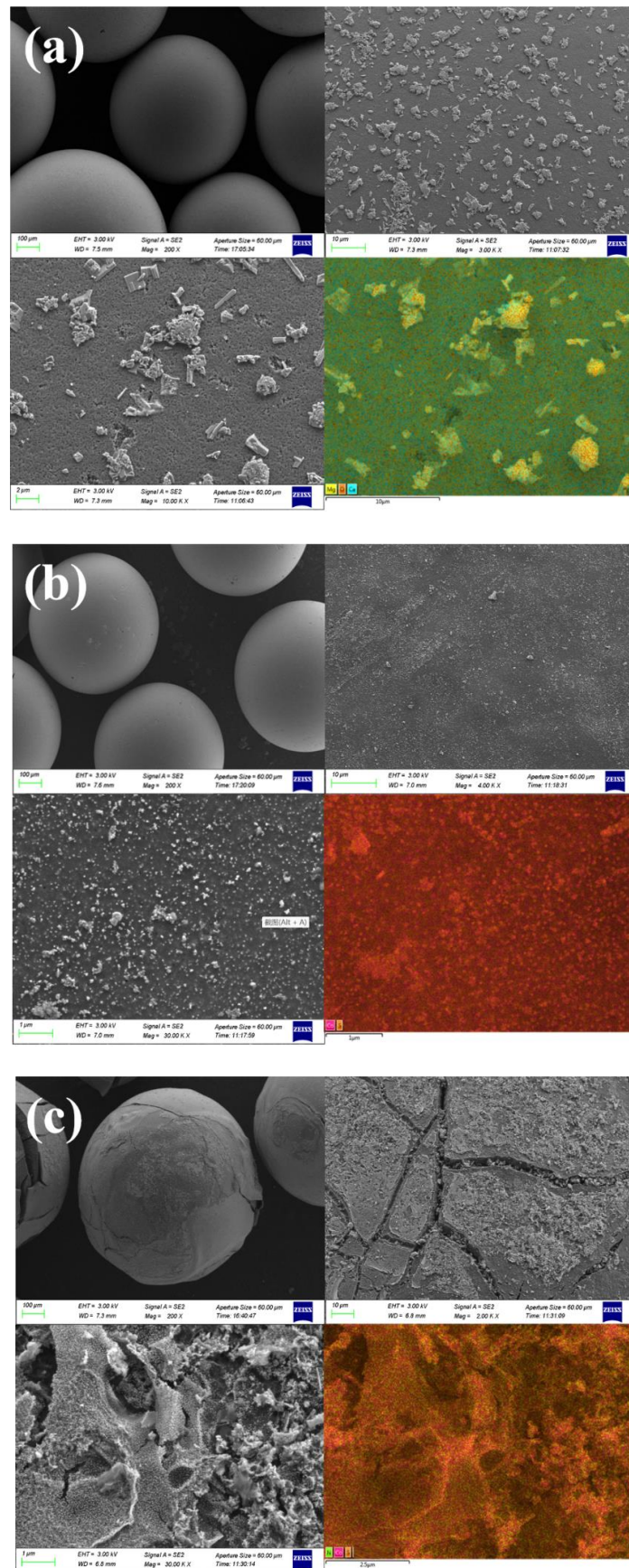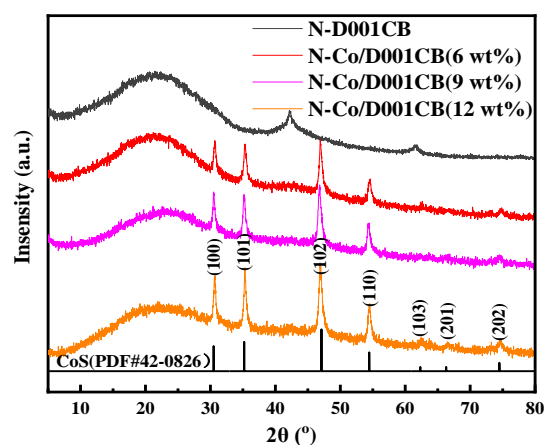
**Figure 1.** SEM and related EDS element layered images of D001CB (**a**); Co/D001CB (**c**); and N-Co/D001CB (**c**).
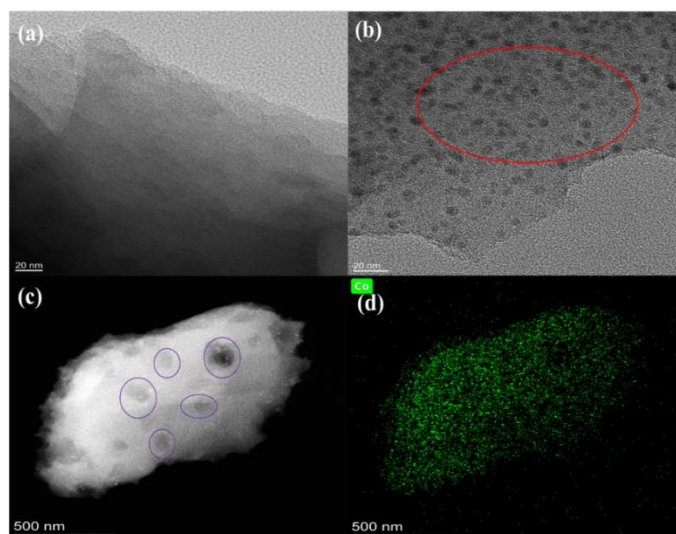
Figure 2. TEM diagrams of D001CB (**a**); and N-Co/D001CB (**b**); EDS layered mapping diagram of cobalt elements (**c**,**d**).

Figure 3. XRD of a nitrogen-doped carbon ball with different cobalt loadings.

The element valence and content of the prepared N-Co/D001CB were determined by X-ray photoelectron spectroscopy (XPS) and infrared spectroscopy (FT-IR), and the possible chemical bonds or functional groups were determined (Figure S3). After cobalt and nitrogen doping, the obvious peak positions of the material were not modified. That is, all of them have characteristic absorption in similar positions, and stretching vibration peaks appear at 3433 cm^{-1} (O-H), 1580 cm^{-1} (C-C/C=C), 1400 cm^{-1} (C-S), and 1130 cm^{-1}(O-C-O), respectively [32,38]. In Figure 4a, it can be seen that the full spectrum of the binding energy positions of each element in N-Co/D001CB, and most of them are similar to the result of Co/D001CB [26]. Figure 4b–f show the valence binding energy peaks of several main elements in the data graph after data processing on behalf of carbon (C 1 s), nitrogen (N 1 s), oxygen (O 1 s), sulfur (S 2p), and cobalt (Co 2p). The position and area of each binding energy peak of C 1 s (Figure 4b) show that it mainly existed in the form of C-C/C=C [39,40], and at 285.2 eV, it may represent the C-S binding energy [40]. After the resin was mixed and sintered with DCD, nitrogen mainly existed on the carbon balls in three forms (Figure 4c), called pyridinic N, pyrrolic N, and graphitic N, corresponding to the binding energy peak positions at 398.1 eV, 399 eV, and 400.3 eV, respectively [37]. The peak area of O 1 s (Figure 4d) was basically at the place with a binding energy of about 532.1 eV, corresponding to the carbon oxygen bond or oxygen species adsorbed on the surface [40–42]. In Figure 4e, typical peaks of C-S or C=S and C-SO_x appeared at binding energies of about 164.0 eV, 165.0 eV, and 167.8 eV, while there were peaks of

S^{2-} corresponding to S $2p_{3/2}$ and S $2p_{1/2}$ at 161.9 eV and 163.2 eV, respectively [43,44]. The binding energy placed at about 785.1 eV and 802.0 eV may be two vibration peaks generated by X-ray emission, as shown in Figure 4d [45–47]. The Co^{3+} and Co^{2+} of Co $2p_{3/2}$ were observed at 778.5 eV and 780.8 eV, respectively, while 793.6 eV and 797.0 eV corresponded to trivalent cobalt and divalent cobalt in Co $2p_{1/2}$ spin-orbit peaks [48]. By comparing it with the peak area, it was found that the peak area of Co^{2+} is the main part. Combined with the XPS peak splitting results of sulfur, cobalt ions are mainly sintered on carbon spheres in the form of cobalt sulfide.
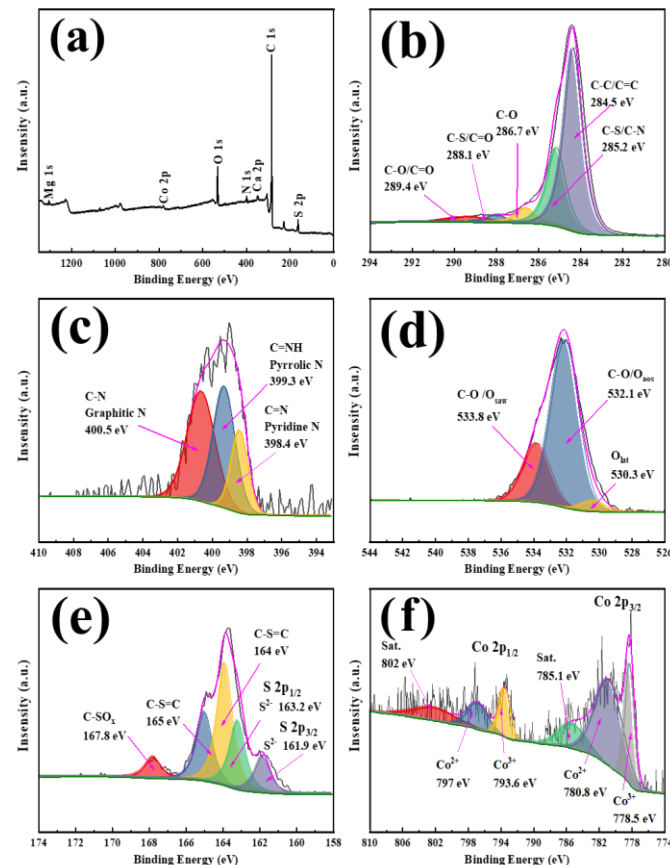
Figure 4. XPS diagram of the main elements of cobalt-doped carbon sphere material, full spectrum of elements (**a**); C 1 s (**b**); N 1 s (**c**); O 1 s (d); S 2p (**e**); Co 2p (**f**).

Finally, the specific surface area, pore volume, and pore size distribution of the carbonized materials were calculated by the nitrogen adsorption and desorption curves (Figure S4), and the main parameters of D001CB, Co/D001CB, and N-Co/D001CB are tabulated in Table 1. It can be found that in the Co/D001CB materials, with the increase in cobalt doping, the specific surface area of the carbon spheres decreased from 31 m^2/g to 7 m^2/g, and the pore volume also decreased significantly, indicating that small particles attached to carbon spheres easily block the pores of carbon spheres. After adding DCD and sintering together to form N-Co/D001CB, this problem can be effectively overcome. As the amount of DCD used increased, the specific surface area greatly improved from 166 m^2/g to 269 m^2/g and nearly increased to 90 m^2/g compared with N-D001CB. Meanwhile, their analyzed pore volumes show a similar trend; the addition of DCD as a nitrogen source for sintering together can significantly improve the relevant BET parameter values of the carbon ball. This means that it is conducive to improving the specific surface area of carbon materials and greatly alleviates the serious shrinkage of the resin frameworks and the blockage of carbon ball pores during resin sintering or contributes to breaking the carbon ball, thereby opening the internal channels, as shown in Figure S1, which helped to increase

the exposure of the catalytic component cobalt sulfide and provides more attachment sites for the reactant.

Table 1. Specific surface area, total pore volume, and pore size of several materials.

| Sample	BET Surface Area (m^2/g)	Total Pore Volume (cm^3/g)	Average Pore Siameter (nm)
Fresh D001 carbon ball	97.6269	0.057726	2.36517
Used D001 carbon ball	67.4460	0.046196	2.73971
Co/D001CB (3 wt%)	31.2506	0.021145	2.70650
Co/D001CB (9 wt%)	22.8031	0.015183	2.66338
Co/D001CB (15 wt%)	6.9895	0.004999	2.86088
N/D001CB (DCD 5 mmol/g)	177.9066	0.113703	2.55646
N-Co/D001CB (DCD 3 mmol/g)	166.3956	0.109752	2.63834
N-Co/D001CB (DCD 5 mmol/g)	269.3317	0.161926	2.43256

3.2. Catalytic Activity of N-Co/D001CB Catalyst

Studies have shown that CoS has the functions of high conductivity, good stability, and affluent active sites to activate PMS. S^{2-} can act as an electron donor to reduce Co^{3+} to Co^{2+}, thus accelerating the electron transfer between the cobalt-based catalyst and PMS and improving its utilization [49,50]. Therefore, it is imperative to explore whether the catalytic effect of nitrogen doping has improved. The degradation ability of IBU with the help of different carbonized catalysts and PMS is shown in Figure 5. It can be seen from different reaction systems that only under the catalyst of Co/D001CB and N-Co/D001CB can significantly activate PMS to degrade IBU. The removal rate of ibuprofen can reach 95% after 60 min under the optimal catalyst of N-Co/D001CB higher than that of Co/D001CB, while the removal rate is less than 15% under the PMS system. The kinetic analysis of the degradation process clearly shows that it followed the first-order reaction kinetic equation (Figure 5b), as well as other kinds of N-Co/D001CB. Next, the catalytic effect of cobalt impregnation with a certain amount of DCD mixed on the properties of N-Co/D001CB was discussed. When the cobalt impregnation amount reaches 0.75 mmol in every gram of D001 resin, the degradation rate of ibuprofen can exceed 95% in one hour, and increasing the cobalt amount not only had an unconsidered catalytic effect (Figure 5c) but also caused a large residue of cobalt ions in the impregnation process. Therefore, this loading amount was the best, and its mass fraction was calculated to be 9% according to the mass of cobalt ions and carbon balls through weighing and theoretical calculations. Similarly, according to the results of different DCD mixed quantities (Figure 5d), 5 mmol was the optimal DCD mixing amount. The corresponding catalyst was used for subsequent activity and mechanism analysis.

The effects of reaction conditions on IBU degradation under the N-Co/D001CB and PMS systems are displayed in Figure 6, and the corresponding fitting results are shown in Figure S5 to acquire the kinetic constants of the reaction conditions. In the identical conditions of the other variables, with increasing catalyst loading, PMS concentration, and temperature, the removal rate of IBU increased. Under optimal conditions, the maximum kinetic constant (k) was more than 0.048 min^{-1}. Meanwhile, according to the activation energy (Ea) calculation formula, it can be found that the logarithmic value of the kinetic constant (lnk) has a linear relationship with the reciprocal of the Kelvin temperature (1/T), and the slope was −Ea/R, R = 8.314 J/(mol·K), so the activation energy of the reaction can be calculated. The fitting result is shown in Figure S6, and the calculated activation energy is 51 kJ/mol, which demonstrates that the intrinsic chemical reaction rate on the surface of N-Co/D001CB plays a dominant role in the apparent reaction rate of the system. Among all the studied factors, the degradation process was greatly affected by the pH value. Significantly, the pH value of the raw solution was 4.5, and the pH value was adjusted through diluted phosphoric acid and sodium hydroxide solutions to study the factors affecting the pH value (Figure 6c). When the pH values were 7 and 9, the degradation rates
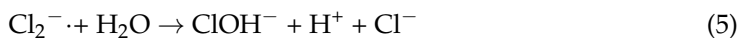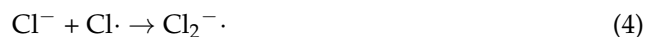
both decreased apparently, possibly because the increase in pH value destroyed a certain carboxyl structure, which was not conducive to generating easily degradable intermediates. When the pH value was 3 or 11, the degradation rate of IBU was significantly inhibited, and the k values were 0.023 min^{-1} and 0.013 min^{-1}, respectively. According to related research, under acidic conditions, the ionization of PMS will be suppressed [21,36], and can quench some free radicals [19]. Under alkaline conditions, the produced $SO_4^-\cdot$ can react with OH^- to produce low activity $\cdot OH$ (Equations (4) and (11)) [51].
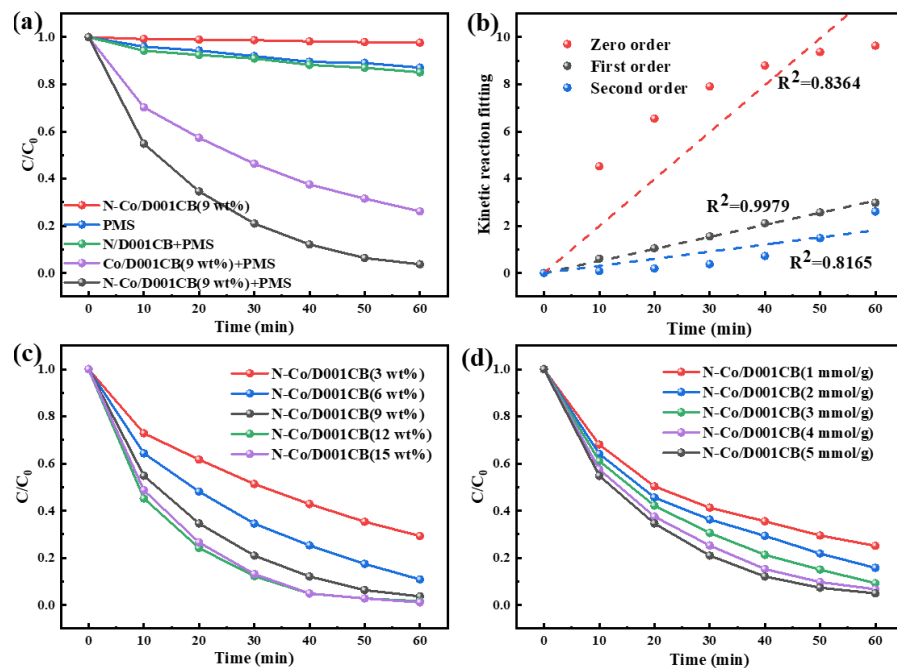

Figure 5. The removal of ibuprofen with different reaction systems (**a**); kinetic fitting curve of N-Co/D001CB + PMS reaction system (**b**); cobalt loading amount (**c**); dicyandiamide amount (**d**); (Temperature = 25 °C, pH = 4.5, PMS = 0.7 mM, amount of catalyst added = 0.3 g/L, IBU = 10 mg/L).

Based on the above reaction conditions, the effects of different concomitant anions were studied, and different concentrations of HCO_3^-, $H_2PO_4^-$, SO_4^{2-}, and Cl^- were discussed in the reaction system (Figure 7). The low concentration of bicarbonate ions inhibited the reaction and showed greater inhibition with increasing concentrations. The detection of the pH value and the comparison with the previous pH value influence experiment may be affected by increasing the pH value of water, or the HCO_3^- may consume the $SO_4^-\cdot$ and generate HCO_3^- as Equations (1) and (2) show [52,53]. With the addition of $H_2PO_4^-$, it had no obvious inhibition of the degradation process. However, SO_4^{2-} had a certain degree of inhibitory effect on the reaction system. Combined with relevant studies, it can be explained that the existence of SO_4^{2-} will inhibit the formation of SO_4^{2-} by HSO_5^-, which will indirectly reduce the formation rate of $\cdot OH$ or $\cdot O_2^-$, as shown in reactions 5 and 7 [54]. In contrast to the first three, the influence of Cl^- was extremely obvious, the inhibition rate was more than 60%, and the kinetic constants were all lower than 0.075 min^{-1}, as shown in Figure S7d. This may be because the PMS concentration in the reaction system was only 0.7 mM, while the concentration of Cl^- exceeds 1 mM. Under these conditions, SO_4^{2-} or HSO_5^- preferentially react with Cl^- to generate $Cl\cdot$ with low oxidation performance, or its ability to degrade organics is poor [31]. The reaction formulas are shown in Equations (3)–(5) [52].

$$HCO_3^- + SO_4^-\cdot \rightarrow HCO_3\cdot + SO_4^{2-} \tag{1}$$

$$HCO_3^- + \cdot OH \rightarrow CO_3\cdot + H_2O \tag{2}$$

$$Cl^- + SO_4^- \cdot \rightarrow Cl \cdot + SO_4^{2-} \tag{3}$$

$$Cl^- + Cl \cdot \rightarrow Cl_2^- \cdot \tag{4}$$

$$Cl_2^- \cdot + H_2O \rightarrow ClOH^- + H^+ + Cl^- \tag{5}$$

The stability of the catalyst material is a crucial index for investigation, especially for tangible materials that are easily separated from water. It is imperative to study the leaching or dissolution of cobalt ions and the recyclability of the material during the experiment. Figure S10 shows the catalytic effect of N-Co/D001CB after five runs and the cobalt ion leaching in each run when the catalyst was fully washed, dried, and calcined at 550 °C for 1 h to recover its active sites. It can be seen that after five operations, the degradation rate of IBU in one hour was 77% in the fifth run, and the catalytic performance of the material declined in the second run was serious. With the use of materials 5 times, the cobalt ion leaching also gradually decreased from 0.47 mg/L to 0.22 mg/L lower than the maximum solubility of cobalt ions in surface water (1 mg/L, GB 38382002), proving that the loss of the cobalt component on the material was the main reason for the reduction of catalytic effect, and the prepared carbon ball catalyst had great recycling ability.
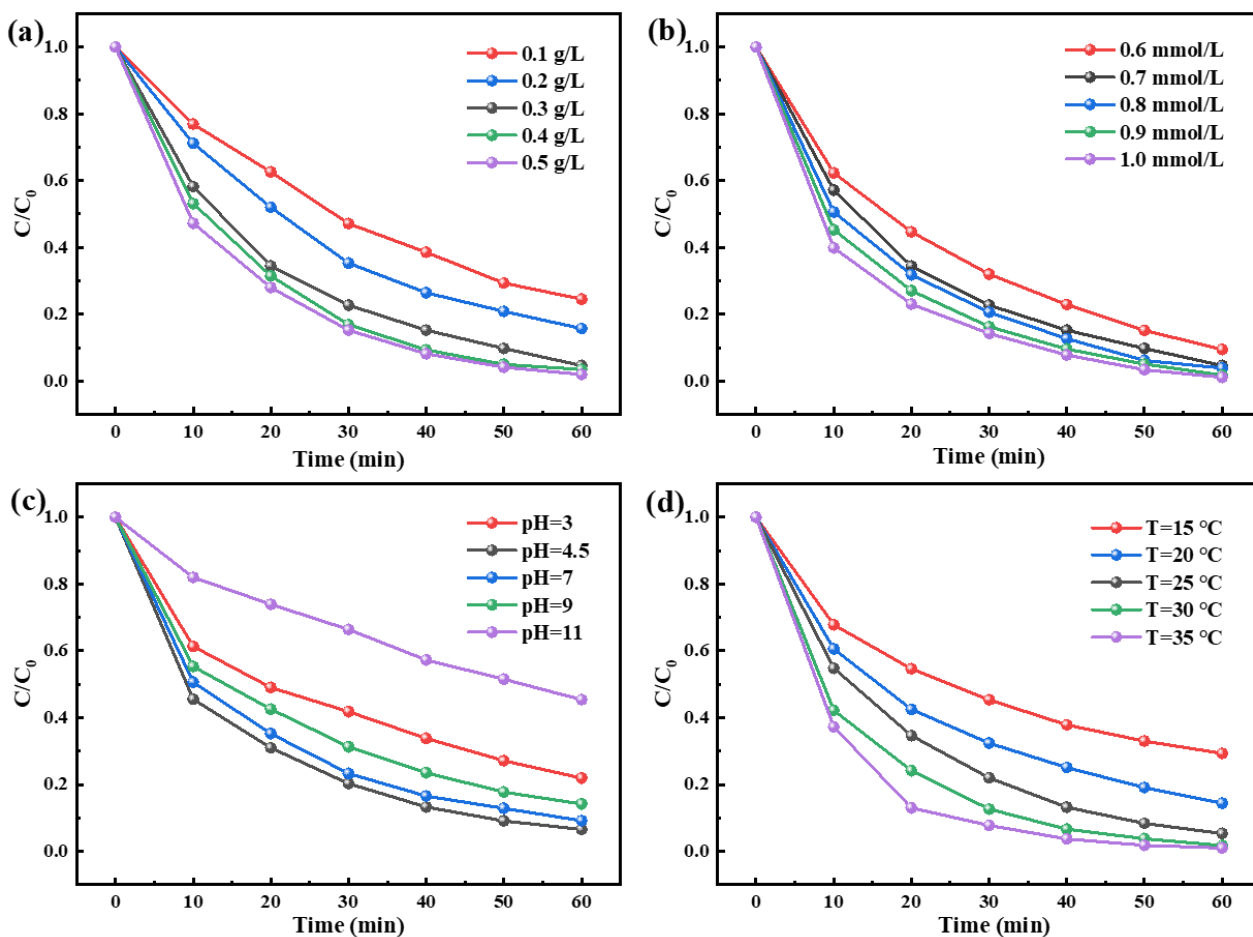
Figure 6. (**a**) The influence of catalyst (Temperature = 25 °C, pH = 4.5, PMS = 0.7 mM, IBU = 10 mg/L); (**b**) The influence of PMS (Temperature = 25 °C, pH = 4.5, catalyst = 0.3 g/L, IBU = 10 mg/L); (**c**) The influence of pH (Temperature = 25 °C, PMS = 0.7 mM, catalyst = 0.3 g/L, IBU = 10 mg/L); (**d**) The influence of temperature (pH = 4.5, PMS = 0.7 mM, catalyst = 0.3 g/L, IBU = 10 mg/L) on the removel of ibuprofen.
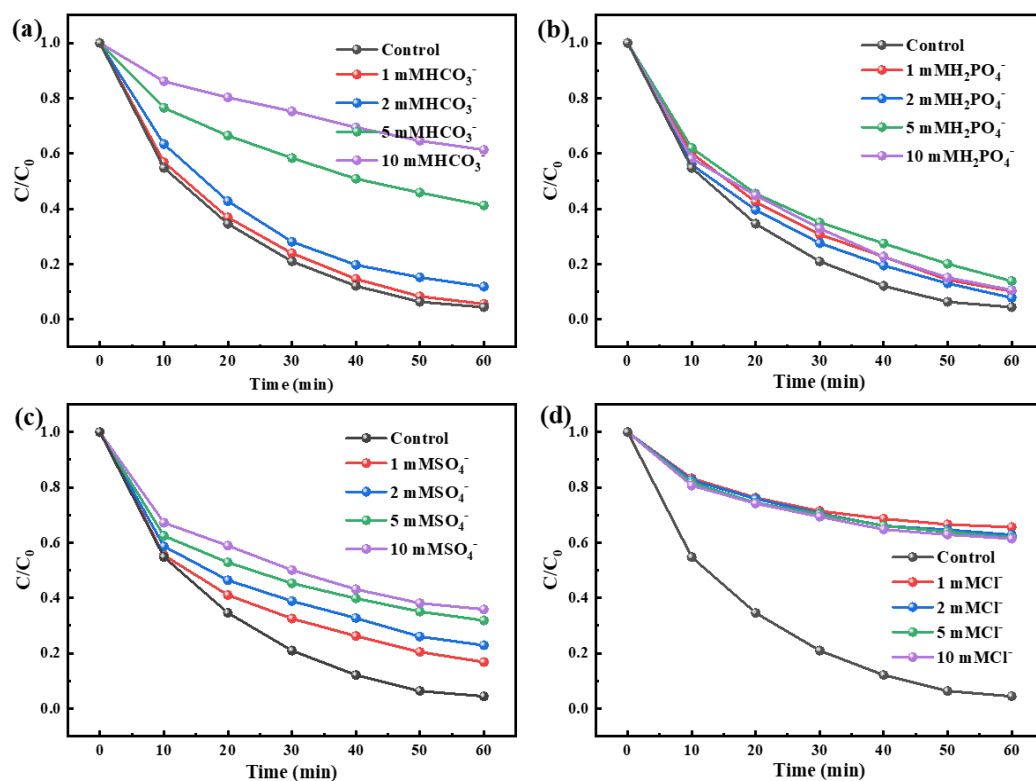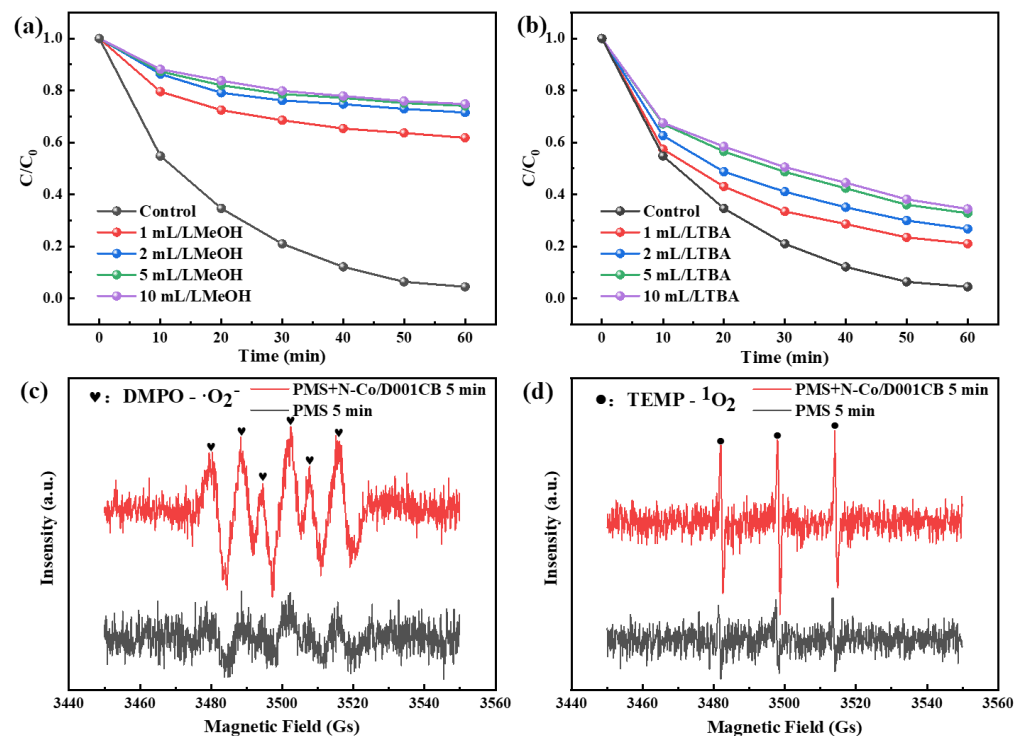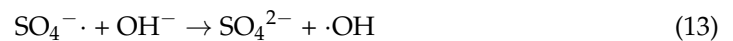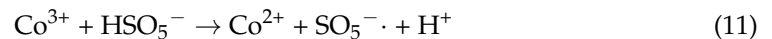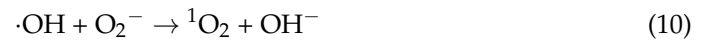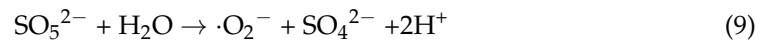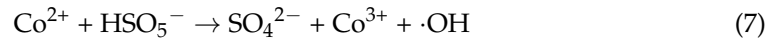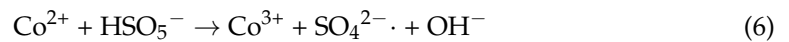
Figure 7. The effects of different concentrations of coexisting anions HCO_3^- (**a**); $H_2PO_4^-$ (**b**); SO_4^{2-} (**c**); and Cl^- (**d**) on the degradation effect of ibuprofen (temperature = 25 °C, pH = 4.5, PMS concentration = 0.7 mM, catalyst loading = 0.3 g/L, IBU concentration = 10 mg/L).

3.3. Mechanism Exploration of Ibuprofen Degradation

To confirm the reactive component in the PMS activation system supported by N-Co/D001CB, radical or nonradical quenching experiments were implemented. In Figure 8a, it can be seen that, by adding MeOH to the experiment, the removel rate of IBU was reduced with an extremely low k value of 0.0044 min^{-1}, which means that the removel of IBU is basically supported by $SO_4^-\cdot$ and $\cdot OH$ [20,36,52], and the effect of $SO_4^-\cdot$ was greater than that of $\cdot OH$ compared with the quenching effect of TBA, with the lowest k value being 0.0165 min^{-1} much higher than 0.0044 min^{-1}, as shown in Figure 8b, while the other two had no distinct effect on the experiment process. This suggests that cobalt sulfide (on the surface of the carbon sphere) has reacted with the HSO_5^- ionized by PMS to form a mass of $SO_4^-\cdot$ and $\cdot OH$. The concerned reaction formulas are 6 and 7 [8], and may be the $SO_4^-\cdot$ generated by the reaction, accounting for the majority, or its redox potential exceeding $\cdot OH$ [7]. Unfortunately, the addition of p-BQ and L-his or FFA to quench the $\cdot O_2^-$ and $^1O_2$ respectively, had an impact on the determination of IBU by HPLC and other testing methods (Figure S11). When they were added to the reaction system, the absorbance of IBU was both greatly affected, resulting in a huge chromatographic peak, causing serious fluctuations in the determination results of the peak area of IBU, and the addition of L-his had a significant inhibition to the reaction, which did not indicate the inhibition of $^1O_2$, but L-his may react with PMS instead [32,52]. Therefore, the EPR was selected to identify and estimate them. The characteristic EPR spectrum adduct signals of DMPO—O_2^- and TEMP—$^1O_2$ were observed both in the different systems at 5 min reaction time, and the signal intensity was increased when the catalyst was added (Figure 8c,d), which proves that they were also generated in the reaction system with poor contributions to the degradation of IBU. The reason for the improved degradation efficiency of IBU is that the introduction

of a catalyst promotes the formation of $SO_4^-\cdot$ and $\cdot OH$ [52]. The relevant possible reactions shown in Equations (6)–(14) [54–56], which had been described in previous studies [26]:

$$Co^{2+} + HSO_5^- \rightarrow Co^{3+} + SO_4^{2-}\cdot + OH^- \tag{6}$$

$$Co^{2+} + HSO_5^- \rightarrow SO_4^{2-} + Co^{3+} + \cdot OH \tag{7}$$

$$HSO_5^- \rightarrow SO_5^{2-} + H^+ \tag{8}$$

$$SO_5^{2-} + H_2O \rightarrow \cdot O_2^- + SO_4^{2-} + 2H^+ \tag{9}$$

$$\cdot OH + O_2^- \rightarrow {}^1O_2 + OH^- \tag{10}$$

$$Co^{3+} + HSO_5^- \rightarrow Co^{2+} + SO_5^-\cdot + H^+ \tag{11}$$

$$2SO_5^-\cdot \rightarrow 2SO_4^- + O_2 \tag{12}$$

$$SO_4^-\cdot + OH^- \rightarrow SO_4^{2-} + \cdot OH \tag{13}$$

$$IBU + SO_4^-\cdot/\cdot OH/\cdot O_2^-/{}^1O_2 \rightarrow Oxidation products \tag{14}$$

Figure 8. The influence of MeOH (**a**); and TBA (**b**) on the catalytic degradation of ibuprofen. EPR test with DMPO or TEMP to detect $\cdot O_2^-$ (**c**); and ${}^1O_2$ (**d**) in the reaction system (temperature = 25 °C, pH = 4.5, PMS concentration = 0.7 mM, catalyst added = 0.3 g/L, IBU concentration = 10 mg/L).

In the IBU degradation path analysis, a substance with a large molecular weight formed and continuously degraded into small molecules according to the liquid chromatography of the reaction water sample every 20 min (Figure S12a). Meanwhile, the substantial reduction in the total peak area indicates that small molecular substances can gradually develop into CO_2 and H_2O. However, the product cannot be mostly mineralized due to its high detected degradation rate, with less than half the mineralization rate. To explore the possible degradation path, the water sample after 20 min of reaction was analyzed by LC-MS analysis, and the results are shown in Figure S12b–f. According to the corresponding mass charge ratio (*m*/*z*) and the relevant literature [4,21], the possible degradation intermediates were approximately speculated (Figure 9). The results showed that hydroxylation, decarboxylation, and demethylation were dominant in the degradation

of IBU. Then, the removed parts can eventually become CO_2 and H_2O. Based on the above discussion, the main prepared steps of N-Co/D001CB and the degradation process of IBU by activating PMS are shown in Figure 10 [8]. In general, after absorbing cobalt ions by impregnation and adding a DCD mixed, the resin was carbonized into a black carbon ball. In the reaction system, N-Co/D001CB had an efficient ability to activate PMS to generate a mass of $SO_4^-\cdot$ and $\cdot OH$, and IBU turned into micromolecule-substances, CO_2 and H_2O, other active substances generated from PMS may play a small role.
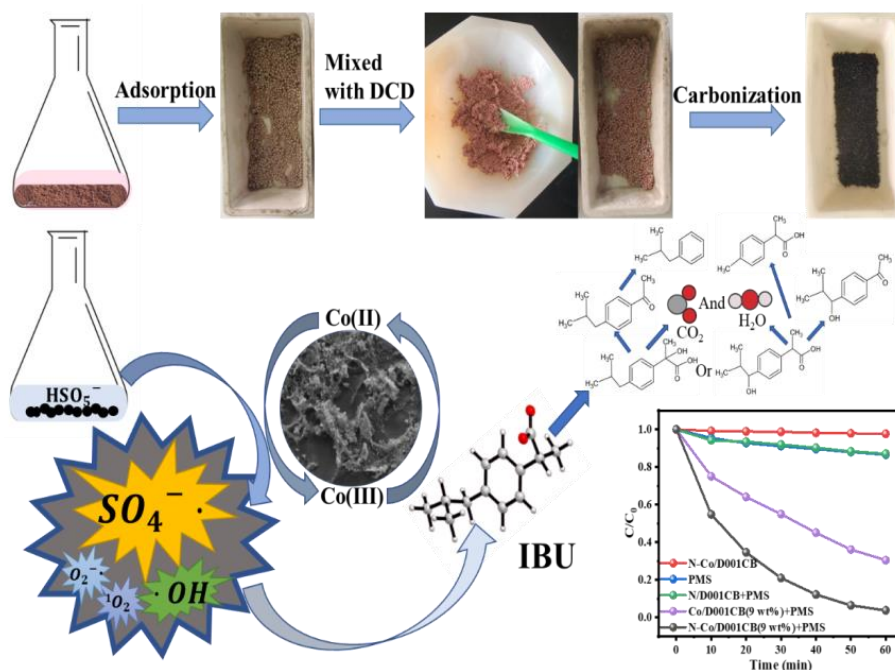

Figure 9. Roadmap for the material preparation step and the degradation process of ibuprofen by activating PMS.
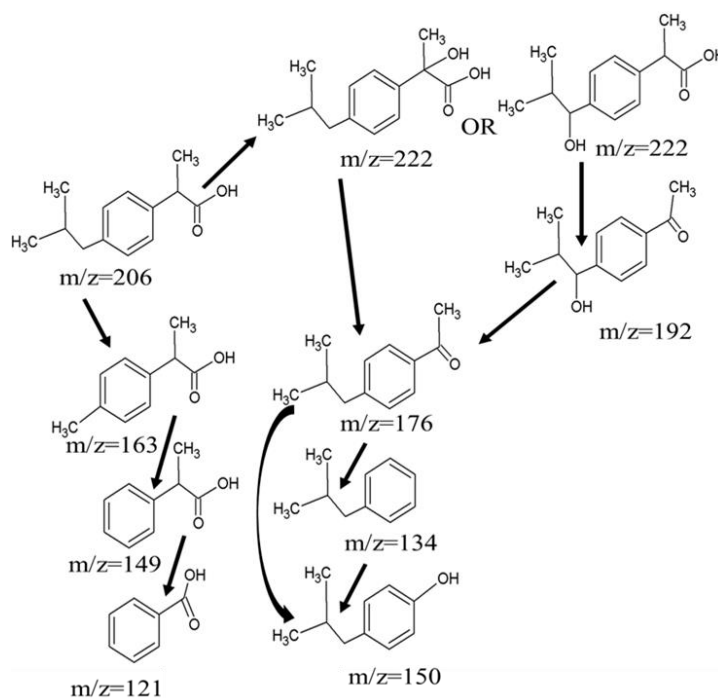

Figure 10. Possible degradation path of IBU in this reaction.

4. Conclusions

The metal cobalt was fixed on the used D001 resin by simple impregnation, mixed with a certain amount of DCD, and then sintered into black carbon balls under high-temperature sintering called N-Co/D001CB. The characterization of XRD and XPS indicated that cobalt was successfully attached to the carbon ball, with the high crystallinity of cobalt sulfide. In particular, DCD as the introduction of a nitrogen source, the BET-related parameters of the materials were significantly improved, and it may greatly alleviate the skeleton shrinkage and pore blockage of carbon ball in the calcination process of cobalt alone and is conducive to the exposure of cobalt sites. In terms of material activity, the degradation rate of IBU can be greatly improved compared with cobalt alone, and the reaction process followed quasi-first-order kinetic equation fitting. The increase in catalyst loading, PMS concentration, and temperature can promote the degradation system, but the pH value and the existence of several common anions have complex impacts. The efficient degradation process of IBU is mainly due to the function of $SO_4^-\cdot$ and $\cdot OH$ produced by activated PMS with the support of N-Co/D001CB according to the quenching experiments. This study provides a potential option for the reuse of D001CB in AOPs, which is easy to separate and recycle. In particular, the carbon balls calcined by adding nitrogen-containing components have a reference value for the preparation of high-activity catalysts.

References

1. de Sousa, D.N.R.; Insa, S.; Mozeto, A.A.; Petrovic, M.; Chaves, T.F.; Fadini, P.S. Equilibrium and kinetic studies of the adsorption of antibiotics from aqueous solutions onto powdered zeolites. *Chemosphere* **2018**, *205*, 137–146. [CrossRef] [PubMed]
2. Oyekunle, D.T.; Wu, B.; Luo, F.; Ali, J.; Chen, Z. Synergistic effects of Co and N doped on graphitic carbon as an in situ surface-bound radical generation for the rapid degradation of emerging contaminants. *Chem. Eng. J.* **2021**, *421*, 129818. [CrossRef]
3. Cao, J.; Yang, Z.H.; Xiong, W.P.; Zhou, Y.Y.; Wu, Y.; Jia, M.Y.; Sun, S.W.; Zhou, C.Y.; Zhang, Y.R.; Zhong, R.H. Peroxymonosulfate Activation of Magnetic Co Nanoparticles Relative to an N-Doped Porous Carbon Under Confinement: Boost-ing Stability and Performance. *Sep. Purif. Technol.* **2020**, *250*, 117237. [CrossRef]
4. Brillas, E. A critical review on ibuprofen removal from synthetic waters, natural waters, and real wastewaters by advanced oxidation processes. *Chemosphere* **2022**, *286*, 131849. [CrossRef] [PubMed]
5. Aziz, K.; Miessner, H.; Mueller, S.; Kalass, D.; Moeller, D.; Khorshid, I.; Rashid, M. Degradation of Pharmaceutical Diclofenac and Ibuprofen in Aqueous Solution, a Direct Comparison of Ozonation, Photocatalysis, and Non-Thermal Plasma. *Chem. Eng. J.* **2017**, *313*, 1033–1041. [CrossRef]
6. Sun, S.P.; Zeng, X.; Lemley, A.T. Nano-Magnetite Catalyzed Heterogeneous Fenton-Like Degradation of Emerging Con-taminants Carbamazepine and Ibuprofen in Aqueous Suspensions and Montmorillonite Clay Slurries at Neutral pH. *J. Mol. Catal. A Chem.* **2013**, *371*, 94–103. [CrossRef]
7. Lee, Y.; Lee, S.; Cui, M.C.; Ren, Y.M.; Park, B.; Ma, J.J.; Han, Z.C.; Khim, J. Activation of Peroxodisulfate and Peroxymono-sulfate by Ultrasound with Different Frequencies: Impact On Ibuprofen Removal Efficient, Cost Estimation and Energy Analysis. *Chem. Eng. J.* **2021**, *413*, 127487. [CrossRef]

8. Wu, X.; Sun, D.; Ma, H.; Ma, C.; Zhang, X.; Hao, J. Activation of peroxymonosulfate by magnetic CuFe$_2$O$_4$@ZIF-67 composite catalyst for the study on the degradation of methylene blue. *Colloids Surfaces A* **2022**, *637*, 128278. [CrossRef]

9. Naderi, M.; Soltani, R.D.C. Hybrid of ZnFe layered double hydroxide/nano-scale carbon for activation of peroxymonosulfate to decompose ibuprofen: Thermodynamic and reaction pathways investigation. *Environ. Technol. Innov.* **2021**, *24*, 101951. [CrossRef]

10. Zheng, X.; Niu, X.; Zhang, D.; Lv, M.; Ye, X.; Ma, J.; Lin, Z.; Fu, M. Metal-based catalysts for persulfate and peroxymonosulfate activation in heterogeneous ways: A review. *Chem. Eng. J.* **2022**, *429*, 132323. [CrossRef]

11. Zeng, H.X.; Deng, L.; Zhang, H.J.; Zhou, C.; Shi, Z. Development of Oxygen Vacancies Enriched Coal Hydrox-ide@Hydroxysulfide Hollow Flowers for Peroxymonosulfate Activation: A Highly Efficient Singlet Oxygen-Dominated Oxidation Process for Sulfamethoxazole Degradation. *J. Hazard. Mater.* **2020**, *400*, 123297. [CrossRef] [PubMed]

12. Peng, Y.H.; Xie, G.S.; Shao, P.H.; Ren, W.; Li, M.L.; Hu, Y.F.; Yang, L.M.; Shi, H.; Luo, X.B. A Comparison of Smx Degra-dation by Persulfate Activated with Different Nanocarbons: Kinetics, Transformation Pathways, and Toxicity. *Appl. Catal. B Environ.* **2022**, *310*, 121345. [CrossRef]

13. Shahzad, A.; Ali, J.; Ifthikar, J.; Aregay, G.G.; Zhu, J.Y.; Chen, Z.L.; Chen, Z.Q. Non-Radical Pms Activation by the Nano-hybrid Material with Periodic Confinement of Reduced Graphene Oxide (RGO) and Cu Hydroxides. *J. Hazard. Mater.* **2020**, *392*, 122316. [CrossRef] [PubMed]

14. Zhao, C.H.; Shao, B.B.; Yan, M.; Liu, Z.F.; Liang, Q.H.; He, Q.Y.; Wu, T.; Liu, Y.; Pan, Y.; Huang, J.; et al. Activation of Peroxymonosulfate by Biochar-Based Catalysts and Applications in the Degradation of Organic Contaminants: A Review. *Chem. Eng. J.* **2021**, *416*, 128829. [CrossRef]

15. Wang, S.; Liu, H.; Wang, J. Nitrogen, sulfur and oxygen co-doped carbon-armored Co/Co$_9$S$_8$ rods (Co/Co$_9$S$_8$@N-S-O-C) as efficient activator of peroxymonosulfate for sulfamethoxazole degradation. *J. Hazard. Mater.* **2020**, *387*, 121669. [CrossRef]

16. Ding, Y.; Wang, X.; Fu, L.; Peng, X.; Pan, C.; Mao, Q.; Wang, C.; Yan, J. Nonradicals induced degradation of organic pollutants by peroxydisulfate (PDS) and peroxymonosulfate (PMS): Recent advances and perspective. *Sci. Total Environ.* **2021**, *765*, 142794. [CrossRef]

17. Kohantorabi, M.; Moussavi, G.; Giannakis, S. A Review of the Innovations in Metal And Carbon-Based Catalysts Explored for Heterogeneous Peroxymonosulfate (Pms) Activation, with Focus On Radical vs. Non-Radical Degradation Pathways of Organic Contaminants. *Chem. Eng. J.* **2021**, *411*, 127957. [CrossRef]

18. Wang, L.L.; Guo, X.; Chen, Y.Y.; Ai, S.S.; Ding, H.M. Cobalt-Doped G-C$_3$N$_4$ as a Heterogeneous Catalyst for Photo-Assisted Activation of Peroxymonosulfate for the Degradation of Organic Contaminants. *Appl. Surf. Sci.* **2019**, *467*, 954–962. [CrossRef]

19. Wang, Z.; Wang, Z.; Li, W.; Lan, Y.; Chen, C. Performance Comparison and Mechanism Investigation of Co$_3$O$_4$-Modified Different Crystallographic Mno2 (A, B, Γ, and Δ) as an Activator of Peroxymonosulfate (Pms) for Sulfisoxazole Degradation. *Chem. Eng. J.* **2022**, *427*, 130888. [CrossRef]

20. Wang, S.; Hu, J.; Wang, J. Degradation of sulfamethoxazole using PMS activated by cobalt sulfides encapsulated in nitrogen and sulfur co-doped graphene. *Sci. Total Environ.* **2022**, *827*, 154379. [CrossRef]

21. Ma, M.; Chen, L.; Zhao, J.; Liu, W.; Ji, H. Efficient activation of peroxymonosulfate by hollow cobalt hydroxide for degradation of ibuprofen and theoretical study. *Chin. Chem. Lett.* **2019**, *30*, 2191–2195. [CrossRef]

22. Zhu, M.; Yang, J.E.; Duan, X.; Wang, S.; Sun, D.D.; Yuan, B.; Fu, M. Engineered Co$_2$AlO$_4$/CoAl$_2$O$_4$@Al$_2$O$_3$ Monolithic Cata-lysts for Peroxymonosulfate Activation: Co^{3+}/Co^{2+} and Odefect/Olattice Ratios Dependence and Mechanism. *Chem. Eng. J.* **2021**, *409*, 128162. [CrossRef]

23. Yu, Y.; Li, N.; Wang, C.; Cheng, Z.; Yan, B.; Chen, G.; Hou, L.; Wang, S. Iron cobalt and nitrogen co-doped carbonized wood sponge for peroxymonosulfate activation: Performance and internal temperature-dependent mechanism. *J. Colloid Interface Sci.* **2022**, *619*, 267–279. [CrossRef]

24. Li, W.; Li, Y.; Wang, H.; Cao, Y.; Yu, H.; Peng, F. Co$_9$S$_8$-porous carbon spheres as bifunctional electrocatalysts with high activity and stability for oxygen reduction and evolution reactions. *Electrochim. Acta* **2018**, *265*, 32–40. [CrossRef]

25. Li, Q.; Song, H.; Ye, Y.; Pan, F.; Zhang, D.; Xia, D. A green designed copper-resin composite for highly efficient catalytic reduction of 4-nitrophenol. *Colloids Interface Sci. Commun.* **2021**, *42*, 100407. [CrossRef]

26. Zhou, G.; Xu, Y.; Zhang, X.; Sun, Y.; Wang, C.; Yu, P. Efficient Activation of Peroxymonosulfate by Cobalt Supported Used Resin Based Carbon Ball Catalyst for the Degradation of Ibuprofen. *Materials* **2022**, *15*, 5003. [CrossRef] [PubMed]

27. Chen, S.; Zhang, M.; Zhang, H.; Yan, X.; Xie, J.; Qi, J.; Sun, X.; Li, J. Dicyandiamide-assisted HKUST-1 derived Cu/N-doped porous carbon nanoarchitecture for electrochemical detection of acetaminophen. *Environ. Res.* **2021**, *201*, 111500. [CrossRef]

28. Li, Y.; Ji, C.; Lu, Y.; Wu, L.; Sun, S.; Qu, R.; Sun, C.; Zhang, Y.; Xue, Z. In situ synthesis of carbon/g-C3N4 composites for visible light catalysis by facile one-step pyrolysis of partially formaldehyde-modified dicyandiamide. *Mater. Chem. Phys.* **2018**, *214*, 28–33. [CrossRef]

29. Ding, S.; Zhang, C.; Liu, Y.; Jiang, H.; Chen, R. Selective hydrogenation of phenol to cyclohexanone in water over Pd@N-doped carbons derived from ZIF-67: Role of dicyandiamide. *Appl. Surf. Sci.* **2017**, *425*, 484–491. [CrossRef]

30. Yang, L.; Chen, W.; Sheng, C.; Wu, H.; Mao, N.; Zhang, H. Fe/N-codoped carbocatalysts loaded on carbon cloth (CC) for activating peroxymonosulfate (PMS) to degrade methyl orange dyes. *Appl. Surf. Sci.* **2021**, *549*, 149300. [CrossRef]

31. Wang, S.; Wang, J. High Efficient Activation of Peroxymonosulfate by Co$_9$S$_8$ Anchored in N, S, O Co-Doped Carbon Composite for Degradation of Sulfamethoxazole: Effect of Sulfur Precursor and Sulfur Doping Content. *Chem. Eng. J.* **2022**, *434*, 134824. [CrossRef]

32. Han, X.; Zhang, W.; Li, S.; Cheng, C.; Zhou, L.; Jia, Q.; Xiu, G. Efficient activation of peroxymonosulfate by MnS/Fe-MOF hybrid catalyst for sulfadiazine degradation: Synergistic effects and mechanism. *Sep. Purif. Technol.* **2022**, *287*, 120509. [CrossRef]

33. Zhou, X.; Luo, C.; Wang, J.; Wang, H.; Chen, Z.; Wang, S.; Chen, Z. Recycling application of modified waste electrolytic manganese anode slag as efficient catalyst for PMS activation. *Sci. Total Environ.* **2021**, *762*, 143120. [CrossRef]

34. Chung, W.-Y.; Brahma, S.; Hou, S.-C.; Chang, C.-C.; Huang, J.-L. Petroleum waste hydrocarbon resin as a carbon source modified on a Si composite as a superior anode material in lithium ion batteries. *Mater. Chem. Phys.* **2020**, *259*, 124011. [CrossRef]

35. Yu, H.J.; Shang, L.; Bian, T.; Shi, R.; Waterhouse, G.; Zhao, Y.F.; Zhou, C.; Wu, L.Z.; Tung, C.H.; Zhang, T.R. Nitro-gen-Doped Porous Carbon Nanosheets Templated From G-C$_3$N$_4$ as Metal-Free Electrocatalysts for Efficient Oxygen Reduction Reaction. *Adv. Mater.* **2016**, *28*, 5080–5086. [CrossRef]

36. Ding, Y.B.; Hu, Y.; Peng, X.Q.; Xiao, Y.W.; Huang, J. Micro-Nano Structured Cos: An Efficient Catalyst for Peroxymonosulfate Activation for Removal of Bisphenol A. *Sep. Purif. Technol.* **2020**, *233*, 116022. [CrossRef]

37. Wang, Q.; Qu, Z.; Chen, S.; Zhang, D. Metal organic framework derived P-doping CoS@C with sulfide defect to boost high-performance asymmetric supercapacitors. *J. Colloid Interface Sci.* **2022**, *624*, 385–393. [CrossRef]

38. Domga; Karnan, M.; Oladoyinbo, F.; Noumi, G.B.; Tchatchueng, J.B.; Sieliechi, M.J.; Sathish, M.; Pattanayak, D.K. A Simple, Economical One-Pot Microwave Assisted Synthesis of Nitrogen and Sulfur Co-Doped Graphene for High Energy Supercapacitors. *Electrochim. Acta* **2020**, *341*, 135999. [CrossRef]

39. Wei, J.; Jiang, C.; Chen, B.; Li, X.; Zhang, H. Hollow C/Co$_9$S$_8$ hybrid polyhedra-modified carbon nanofibers as sulfur hosts for promising Li–S batteries. *Ceram. Int.* **2021**, *47*, 25387–25397. [CrossRef]

40. Arunpandian, M.; Selvakumar, K.; Raja, A.; Rajasekaran, P.; Ramalingan, C.; Nagarajan, E.R.; Pandikumar, A.; Arunachalam, S. Rational Design of Novel Ternary Sm$_2$Wo$_6$/Zno/Go Nanocomposites: An Affordable Photocatalyst for the Mitigation of Carcinogenic Organic Pollutants. *Colloids Surfaces A* **2020**, *596*, 124721.

41. Huang, H.; Yang, G.; Yu, J.; Zhang, J.; Xia, Y.; Wang, K.; Liang, C.; Gan, Y.; He, X.; Zhang, W. One-Pot Synthesis of Nano-crystalline Sns@Tremella-Like Porous Carbon by Supercritical Co2 Method for Excellent Sodium Storage Performance. *Electrochim. Acta* **2021**, *373*, 137933. [CrossRef]

42. Jiang, J.B.; Zhu, L.Y.; Sun, Y.X.; Chen, Y.K.; Chen, H.T.; Han, S.; Lin, H.L. Fe$_2$O$_3$ Nanocatalysts On N-Doped Carbon Nanomaterial for Highly Efficient Electrochemical Hydrogen Evolution in Alkaline. *J. Power Sources* **2019**, *426*, 74–83. [CrossRef]

43. Liu, X.X.; Wu, R.; Wang, Y.; Xiao, S.H.; He, Q.; Bin Niu, X.; Blackwood, D.J.; Chen, J.S. Self-supported core/shell Co$_3$O$_4$@Ni$_3$S$_2$ nanowires for high-performance supercapacitors. *Electrochim. Acta* **2019**, *311*, 221–229. [CrossRef]

44. Chen, P.; Gou, Y.J.; Ni, J.M.; Liang, Y.M.; Yang, B.Q.; Jia, F.F.; Song, S.X. Efficient Ofloxacin Degradation with Co(Ii)-Doped Mos2 Nano-Flowers as Pms Activator Under Visible-Light Irradiation. *Chem. Eng. J.* **2020**, *401*, 125978. [CrossRef]

45. Ren, X.; Du, Y.Y.; Song, M.Y.; Zhou, Y.H.; Chen, Y.J.; Ma, F.W.; Wan, J.F. In-Situ Transformation of Ni Foam Into Sandwich Nanostructured Co$_{1.29}$Ni$_{1.71}$O$_4$ Nanoparticle@Coni$_2$S$_4$ Nanosheet Networks for High-Performance Asymmetric Supercapacitors. *Chem. Eng. J.* **2019**, *375*, 122063. [CrossRef]

46. Zhang, X.; Wang, J.; Ji, X.; Sui, Y.; Wei, F.; Qi, J.; Meng, Q.; Ren, Y.; He, Y. Nickel/cobalt bimetallic metal-organic frameworks ultrathin nanosheets with enhanced performance for supercapacitors. *J. Alloys Compd.* **2020**, *825*, 154069. [CrossRef]

47. Chen, X.; Li, Y.; Li, C.; Cao, H.L.; Wang, C.Z.; Cheng, S.Y.; Zhang, Q. A Novel Strategy of Multi-Element Nanocomposite Synthesis for High Performance Zno-Cose$_2$ Supercapacitor Material Development. *Chin. J. Chem.* **2021**, *39*, 2441–2450. [CrossRef]

48. Qiu, W.D.; Xiao, H.B.; Yu, M.H.; Li, Y.; Lu, X.H. Surface Modulation of NiCo$_2$O$_4$ Nanowire Arrays with Significantly Enhanced Reactivity for Ultrahigh-Energy Supercapacitors. *Chem. Eng. J.* **2018**, *352*, 996–1003. [CrossRef]

49. Fang, Z.; Qi, J.; Xu, Y.; Liu, Y.; Qi, T.; Xing, L.; Dai, Q.; Wang, L. Promoted generation of singlet oxygen by hollow-shell CoS/g-C$_3$N$_4$ catalyst for sulfonamides degradation. *Chem. Eng. J.* **2022**, *441*, 136051. [CrossRef]

50. Zhou, X.; Luo, M.; Xie, C.; Wang, H.; Wang, J.; Chen, Z.; Xiao, J.; Chen, Z. Tunable S doping from Co$_3$O$_4$ to Co$_9$S$_8$ for peroxymonosulfate activation: Distinguished Radical/Nonradical species and generation pathways. *Appl. Catal. B Environ.* **2020**, *282*, 119605. [CrossRef]

51. Ren, Z.; Romar, H.; Varila, T.; Xu, X.; Wang, Z.; Sillanpää, M.; Leiviskä, T. Ibuprofen degradation using a Co-doped carbon matrix derived from peat as a peroxymonosulphate activator. *Environ. Res.* **2021**, *193*, 110564. [CrossRef] [PubMed]

52. Hou, K.J.; Pi, Z.J.; Chen, F.; He, L.; Yao, F.B.; Chen, S.J.; Li, X.M.; Wang, D.B.; Dong, H.R.; Yang, Q. Peroxymonosulfate (PMS) Activation by Mackinawite for the Degradation of Organic Pollutants: Underappreciated Role of Dissolved Sulfur Derivatives. *Sci. Total Environ.* **2022**, *834*, 151421. [CrossRef] [PubMed]

53. Xu, H.; Jiang, N.; Wang, D.; Wang, L.; Song, Y.; Chen, Z.; Ma, J.; Zhang, T. Improving PMS oxidation of organic pollutants by single cobalt atom catalyst through hybrid radical and non-radical pathways. *Appl. Catal. B Environ.* **2020**, *263*, 118350. [CrossRef]

54. Zhang, Y.; Yang, T.; Li, R.; Cao, X.; Kan, Y.; Wei, B.; Sun, X. Efficient degradation of ibuprofen by Co/Fe@CNFs catalyst in the presence of peroxymonosulfate and persulfate: Characterization, performance, and mechanism comparison. *J. Taiwan Inst. Chem. Eng.* **2022**, *131*, 104161. [CrossRef]

55. Zhang, G.; Ding, Y.; Nie, W.; Tang, H. Efficient degradation of drug ibuprofen through catalytic activation of peroxymonosulfate by Fe3C embedded on carbon. *J. Environ. Sci.* **2019**, *78*, 1–12. [CrossRef]

56. Li, M.; Zhong, H.; He, Z.; Hu, L.; Sun, W.; Loganathan, P.; Xiong, D. Degradation of various thiol collectors in simulated and real mineral processing wastewater of sulfide ore in heterogeneous modified manganese slag/PMS system. *Chem. Eng. J.* **2021**, *413*, 127478. [CrossRef]